Observed Interaction between Low and High Frequency Motions off the Coasts of Peru and California

PIJUSH K. KUNDU

Oceanographic Center, Nova University, Dania, Florida

ROBERT C. BEARDSLEY

Woods Hole Oceanographic Institution, Woods Hole, Massachusetts

ADRIANA HUYER

School of Oceanography, Oregon State University, Corvallis, Oregon

(Manuscript received 13 December 1989, in final form 9 February 1990)

ABSTRACT

Datasets taken near the coasts of Peru and California have been analyzed to explore the evidence of a correlation between the high frequency (period < 10.8 hour) and low frequency (period > 4 day) motions. A large part of the high frequency current is consistent with internal wave dynamics. They have a near 180° phase change across the water column; there is also evidence of a clockwise veering with depth, presumably due to frictional effects. No correlation of the vertical Reynolds stress $\overline{vw}$ and vertical shear V_z is found. The horizontal stress $\overline{uv}$ is found to be negatively correlated with the horizontal shear V_x only when averaged over time and space scales larger than those of the mean velocity field. The implied eddy viscosity is of order $\nu_H \sim 10^5$ cm^2 s^{-1}. It is suggested that the relaxation time for the wave field to lose asymmetry is larger than the time for the wave to propagate across a typical scale of the mean shear field. Due to this the fluctuating field may locally behave like a negative eddy viscosity at certain places.

1. Introduction

A large part of the kinetic energy of oceanic variability is generated at mesoscales, possibly by instabilities. These have periods of weeks, and lengths of a few hundred kilometers. The dissipation of kinetic energy, on the other hand, takes place at the Kolmogorov scale of order a few millimeters. There must therefore be fluctuations which drain energy out of the larger scales (mean) and feed the smaller scales (fluctuations). They are small-scale three-dimensional disturbances, because large-scale two-dimensional disturbances tend to cascade energy in the opposite direction, toward larger scales.

A division into "mean" and "fluctuation" is somewhat arbitrary. One natural division, however, is the Coriolis frequency f, because then the high frequency fluctuations can be attributed to internal waves with $\omega > f$. In fact, Müller (1976, 1977) suggested that internal waves in the ocean behave much like molecules in a gas. In the absence of a mean flow, the internal wave field is in a basic state that is vertically symmetric ($\overline{uw} = \overline{vw} = 0$) and horizontally isotropic ($\overline{uv} = 0$). [Here (u, v, w) are the fluctuating velocity components, and the overbar denotes ensemble average. Lower case letters refer to the fluctuating field, and upper case letters refer to the mean field.] On application of a shear flow, however, the wave field develops asymmetries and anisotropies. Müller speculated that nonlinear interactions between waves of different frequencies and wavenumbers, playing the role of molecular collisions, constantly tend to randomize the wave orientations, so that the wave field can have a relationship with the *local* shear field at a certain point. In the absence of such relaxation effects, the wave field cannot be "aware" of the changes in shear; consequently, the wave field has no relationship with the *local shear*, and there cannot be a net exchange of energy between the mean and fluctuating fields. In fact, the relaxation time τ_R (during which the wave asymmetry decays) needs to be smaller than the propagation time τ_P (the time taken by the wave field to travel one spatial scale of the mean shear field), in order for the wave field to extract energy from the mean field. Kundu et al. (1988) hypothesized that the mechanism of vortex stretching may selectively enhance the energy of the internal waves packets whose phase velocity is oriented along the principal axis of the mean strain field. These in-

Corresponding author address: Dr. Pijush K. Kundu, Oceanographic Center, 800 North Ocean Drive, Nova University, Dania, Florida 33004.

ternal waves have a Reynolds stress $\overline{uv} < 0$ if the mean shear $V_x > 0$, so that the waves extract energy from the mean field, diffuse its spatial gradients, and act as eddy viscosity.

The interaction of the mean shear with fluctuations in the internal-wave frequency range was explored in Kundu et al. (1988) in a dataset taken off the coast of British Columbia. A coastal study has the advantage that only the dominant cross-shore shear of the alongshore mean velocity needs to be considered for estimating the horizontal strain rate. The eddy viscosity hypotheses in the horizontal and vertical planes are respectively expressed as

$$-\overline{u_\alpha u_\beta} = \nu_H\left(\frac{\partial U_\alpha}{\partial x_\beta} + \frac{\partial U_\beta}{\partial x_\alpha}\right) \tag{1}$$

$$-\overline{u_\alpha w} = \nu_v\left(\frac{\partial U_\alpha}{\partial z} + \frac{\partial W}{\partial x_\alpha}\right) \tag{2}$$

where Cartesian tensor notation is used, with α and β denoting horizontal directions. [Since the left side of (1) is symmetric in the indices α and β, the hypothesis in the horizontal plane cannot be written as $-\overline{u_\alpha u_\beta} = \nu_H \partial U_\alpha/\partial x_\beta$, because then the right side of the expression would not be symmetric in α and β; see the discussion in Kundu et al. (1988).] Aligning the coordinate system such that the y-axis points alongshore, the x-axis onshore, and the z-axis upward, (1) and (2) become

$$-\overline{uv} = \nu_H\left(\frac{\partial U}{\partial y} + \frac{\partial V}{\partial x}\right) \approx \nu_H \frac{\partial V}{\partial x} \tag{3}$$

$$-\overline{vw} = \nu_v\left(\frac{\partial V}{\partial z} + \frac{\partial W}{\partial y}\right) \approx \nu_v \frac{\partial V}{\partial z} \tag{4}$$

where U_y has been neglected in (3) because $U \ll V$ and $\delta x \ll \delta y$ near a coast; here δx and δy are the characteristic length scales of the mean flow in the cross-shelf and alongshore directions, respectively. In the open ocean, both U and V tend to be in geostrophic balance, so that the sum $(U_x + V_y)$ is generally a small quantity, leading to considerable errors in its estimation.

No correlation of the time variation of vertical Reynolds stress $\overline{vw}(t)$ and the vertical shear of the alongshore current $V_z(t)$ was found by Kundu et al. (1988). (Here the overbar represents the average over 4 days.) A weak correlation was found between the horizontal shear $V_x(t)$ and the horizontal stress $\overline{uv}(t)$ at one station, but the evidence was not convincing. What was convincing is that the *mean* Reynolds stress (averaged over the *record length*) was of the same sign *everywhere* on a cross section perpendicular to the coast (Fig. 1). However, the sign of the record-average Reynolds stress was found to be unrelated to the local sign of the mean horizontal shear. This is seen in Fig. 2, which shows the offshore structure of the alongshore velocity for the depth range for which there were enough current meters to determine an offshore profile. It is seen that the horizontal shear changes sign in the offshore direction, although the sign of the Reynolds stress in Fig. 1 is uniform. Kundu et al. (1988) did not provide an adequate explanation.

In view of the intriguing but weak evidence of the earlier work, a similar calculation is done here, using datasets collected off the coasts of Peru and California. It is again found that the sign of the mean Reynolds stress is fairly uniform on a section perpendicular to the coast, and is unrelated to the local mean horizontal shear. An explanation for such a behavior is provided in this study.

2. The datasets

Two datasets are used in the present calculation. One of these is part of the measurements made by Oregon State University during the JOINT 2 experiment, off the coast of Peru. These are summarized in the report by Enfield et al. (1978). Only the current and temperature measurements made during the "leg V" (March–May 1977) are used here because of the extensive data coverage in this leg. The mooring positions are shown in Fig. 3, and the instrument depths are indicated in the first column of Table 1. For the sake of brevity, the measurements are referred to by the first three letters of the mooring site, followed by the nominal depth. For example, MIL-39 will designate measurements at 39 m on station Mila.

The second dataset used here is the CODE 2 set, taken off the coast of California during April–August 1982. These are summarized in the data report by Winant et al. (1985); several interesting features of the data are pointed out in Winant et al. (1987). The mooring positions are shown in Fig. 4, and the instrument depths are indicated in the first column of Table 2.

For the Peru data, most of the measurements have a 20 minute sampling interval, but some have a 15 minute interval. In order to have a uniform data interval, the 15 minute measurements are first converted to 20 minute measurements. This is done by finding the Fourier coefficients of the 15 minute time series, omitting the coefficients corresponding to $\omega > 1.5$ cph (= Nyquist frequency corresponding to 20 minute data), and reconstructing the series by recombining the Fourier coefficients. For the CODE 2 data, all measurements were similarly converted to 7.5 minute measurements, from the original 4 minute and 7.5 minute series.

Generally, very little signature of pure inertial oscillations was found in the Peru data (Enfield et al. 1978). However there were a few exceptions, an example of which is shown in Fig. 5a, showing the spectrum at MILA-39. Most CODE stations did have a prominent inertial peak (Fig. 5b). In both datasets there is a strong semidiurnal peak, and a weak diurnal peak.

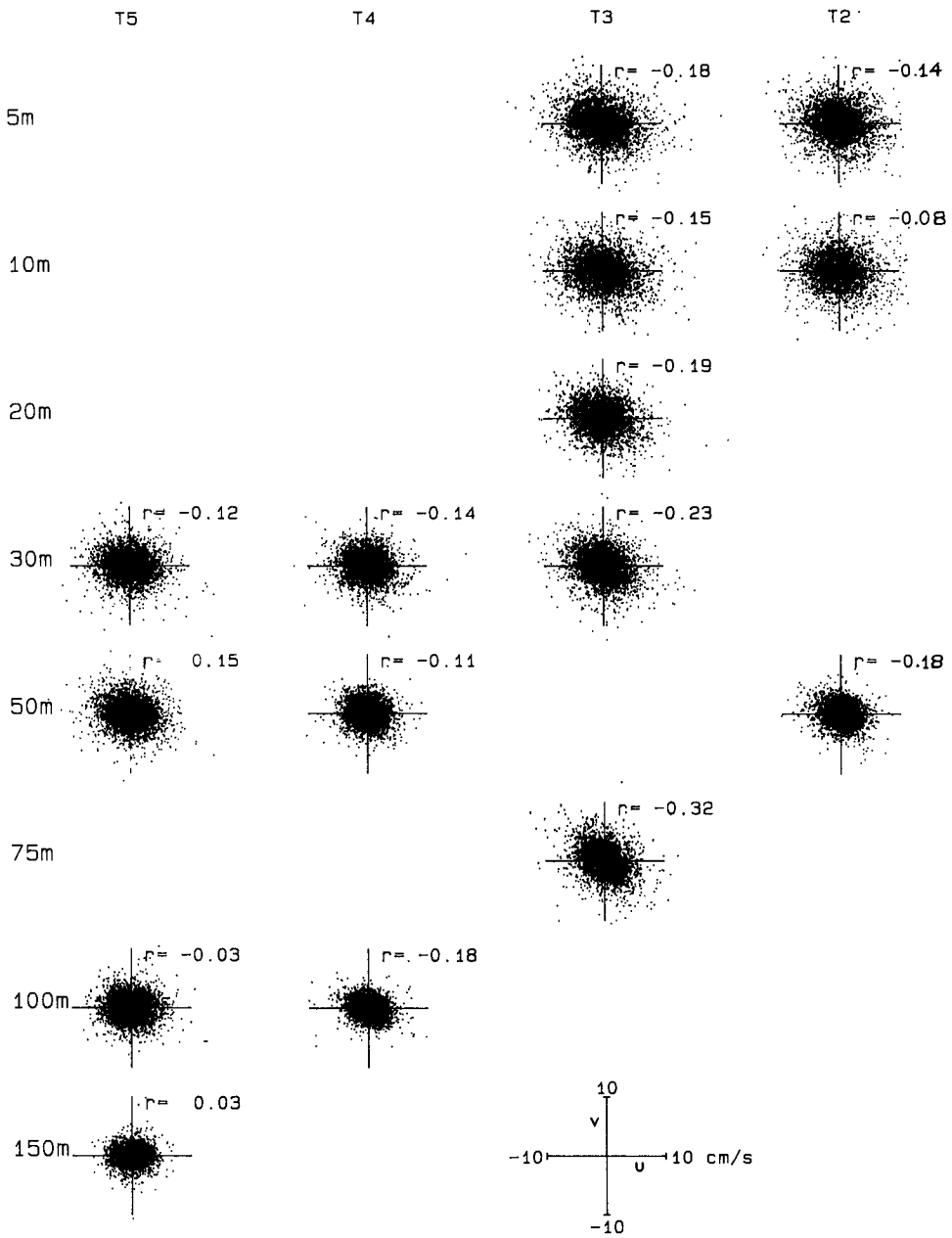

FIG. 1. Scatter plots of high frequency (0.13 cph $< \omega <$ 0.5 cph) horizontal velocity fluctuations in a 4 month long coastal dataset, taken off the coast of British Columbia and analyzed by Kundu et al. (1988). T2, T3, T4 and T5 are station names, with T2 as the nearshore station. The velocity scale is shown in the lower right hand corner. The correlation coefficient r between u and v is recorded alongside each plot. Note that r is negative everywhere, except for a small value of +0.03 near the ocean bottom at T5.

Although the spectra do not always show a valley at frequencies just lower than f, we decided to treat fluctuations with a period larger than 4 days ($\omega < 0.01$ cph) as the low frequency series, as in Kundu et al. (1988). Following previous work on the subject, the high frequency series are designed to retain all frequencies higher than the tides. For the Peru data the frequency range of the high frequency series is 0.092 $< \omega <$ 1.5 cph, and that for the CODE data is 0.125 $< \omega <$ 4.0 cph. (The upper limits of the range are the Nyquist frequencies corresponding to the respective data interval.) The low and high frequency components are extracted from the data by finding the Fourier coefficients, retaining those in the desired frequency range, and reconstructing the time series by Fourier recombination.

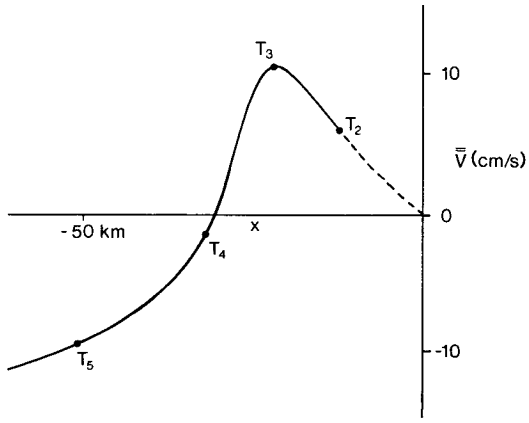

FIG. 2. Offshore structure of mean (average over 4 month record) alongshore velocity in the depth range 30–50 m, in Kundu et al. (1988). Note that the mean shear changes sign, although the mean Reynolds stress in Fig. 1 is always negative.

The currents are then resolved into alongshore and cross-shore directions. Based on direction of the coast and isobaths (Fig. 3), the alongshore direction for the Peru data is chosen to be 40° anticlockwise of north at the three northern moorings (Peyote, Yucca, and Opuntia), and 45° at all other moorings. For the CODE data (Fig. 4), the alongshore direction is chosen to be 43° anticlockwise of north, as in Winant et al. (1987). The x-coordinate is taken towards the coast (close to the NE direction), and the y-coordinate along the coast (close to the NW direction). The corresponding low frequency currents are denoted by $[U(t), V(t)]$, and the high frequency fluctuating currents are denoted by $[u(t), v(t)]$. The 4-day averages are denoted by an overbar. (All fields termed 4-day "averages" in the paper are actually computed by low-pass filtering, and not by taking the arithmetic mean over 4 days.) The Reynolds stresses are therefore denoted by $\overline{uv}(t)$, $\overline{uw}(t)$ and $\overline{vw}(t)$. Averages over the *entire record* are denoted by a double overbar; thus the record-mean alongshore velocity is $\bar{\bar{V}}$, and the record-mean horizontal Reynolds stress is $\overline{\overline{uv}}$.

Vertical velocity is estimated from the temperature series by assuming a strictly advective balance

$$w = -\frac{T_t}{T_z} \tag{5}$$

where T_t and T_z denote the time and vertical derivatives of temperature. The vertical derivative T_z is estimated from low frequency temperature series by finding the difference between two consecutive instruments on the same mooring; T_t is computed by finite differencing the high frequency series. Neglected terms in (5), such as horizontal advection and diffusion, can introduce large errors in the estimates of w; Ruddick and Joyce (1979) discuss these possible errors in some detail. Moreover, the average vertical gradient of temperature determined from the difference of T between two instrument depths may not be indicative of the local T_z, because of the presence of fine structure. Therefore, the w field computed from (5) has to be regarded with caution.

The Reynolds stresses $\overline{uv}$, $\overline{uw}$, and $\overline{vw}$ are computed by multiplying the high frequency components (u, v, w) of the currents, and then computing the 4-day averages of the product series. The present method of estimating Reynolds stress is more direct than that of Frankignoul (1974, 1976), Frankignoul and Joyce (1979) and Ruddick and Joyce (1979), who divided the records into short detrended segments of 3–4 days length, Fourier analyzed them, and integrated the cospectra in the frequency range $(2f, N)$ to obtain the Reynolds stresses for each segment.

3. Nature of the fluctuating motion

Several studies in the *open ocean* indicate that a large part of the observed motion in the frequency range $f < \omega < N$ is indeed consistent with internal wave dynamics (Fofonoff 1969; Gonella 1972). The fluctuating motions studied here are in the internal frequency range. However, this is a coastal region, and the fluctuations are expected to be influenced by the effects of boundary mixing, strong nonlinearity, and Doppler shifting effects. Therefore, there is no a priori reason for these motions to obey internal wave dynamics.

In order to investigate whether the fluctuating motion has symptoms of internal waves, we estimated the "rotary coefficient," defined as

$$C_0 = \frac{2Q_{uv}}{P_{uu} + P_{vv}} \tag{6}$$

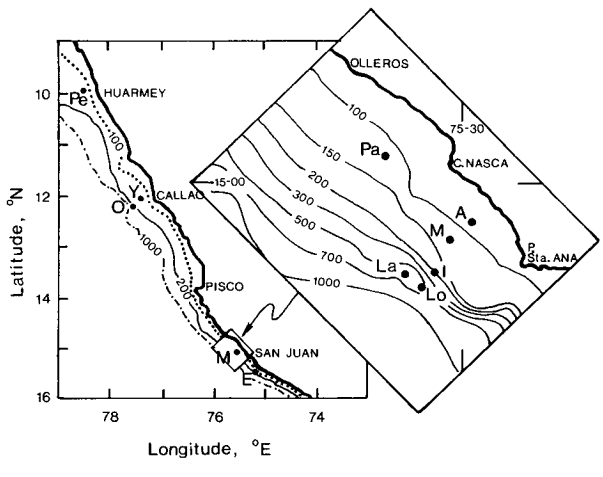

FIG. 3. Locations of current meter moorings near the coast of Peru during the JOINT 2 experiment. Constant depth contours are indicated in meters. The inset shows details near 15°S. Mooring symbols are E: Euphorbia, M: Mila, Y: Yucca, O: Opuntia, Pe: Peyote, A: Agave, I: Ironwood, Lo: Lobivia, La: Lagarta, Pa: Parodia.

TABLE 1. Record-average onshore and alongshore velocity and horizontal Reynolds stress, for the Peru data.

Station–depth (m)	Distance from coast (km)	Water depth (m)	$\bar{\bar{U}}$ (cm s^{-1})	$\bar{\bar{V}}$ (cm s^{-1})	$\frac{\overline{\overline{uv}}}{u_{rms}v_{rms}}$	$\overline{\overline{uv}}$ (cm^2 s^{-2})
PEY-37	20	117	−3.8	−19.4	−0.25	−2.11
PEY-56			−5.2	−21.3	−0.37	−2.11
PEY-96			−5.1	−13.6	−0.20	−0.63
AGA-26	4	86	3.8	−3.1	−0.02	−1.03
AGA-46			5.4	−9.0	−0.10	−1.62
AGA-67			1.4	−6.6	+0.09	+0.54
AGA-77			−0.3	−5.0	+0.02	+0.10
LOB-58	24	580	−1.3	−10.6	−0.18	−1.09
LOB-83			−0.8	−6.4	−0.14	−0.58
LOB-183			−0.2	−4.3	−0.05	−0.28
LOB-283			−0.4	0.5	−0.02	−0.10
LAG-92	24	620	−0.8	−13.0	−0.17	−0.76
LAG-115			−0.8	−11.5	−0.20	−0.88
LAG-224			−0.4	−1.0	−0.07	−0.36
LAG-512			0.7	−1.4	−0.22	−0.70
OPU-224	42	620	−0.4	−2.7	−0.10	−0.39
OPU-324			−0.4	−2.3	−0.21	−1.22
OPU-524			0.2	0.0	−0.14	−0.54
IRO-24	20	205	−4.8	−4.6	0.00	0.00
IRO-44			−0.7	−8.1	−0.06	−1.48
IRO-63			−0.1	−10.7	−0.05	−0.83
IRO-105			−0.5	−10.1	−0.17	−1.60
IRO-155			−1.4	−7.1	−0.09	−0.88
IRO-180			−1.1	−7.0	−0.05	−0.50
EUP-26	7	123	0.6	−0.2	+0.08	+2.38
EUP-63			1.9	−5.3	−0.07	−1.38
PAR-24	10	124	0.7	−2.7	−0.06	−0.78
PAR-64			1.4	−8.8	−0.05	−0.82
PAR-104			−0.2	−3.8	−0.11	−0.59
YUC-37	8	117	−6.0	−8.3	−0.32	−4.65
YUC-57			−2.7	−6.9	−0.25	−1.69
YUC-97			−3.1	−4.5	−0.10	−0.37
MIL-19	12	121	0.7	−3.2	+0.04	+1.30
MIL-39			4.2	−9.1	−0.01	−0.18
MIL-59			5.0	−9.7	0.00	0.00
MIL-80			3.0	−8.7	0.00	0.00
MIL-100			0.7	−6.0	−0.04	−0.41
MIL-115			−1.8	−2.9	−0.08	−0.41

Here P is the cospectra and Q is the quadrature spectra. That is, $P_{uu} = \mathrm{Re}(\tilde{u}^*\tilde{u})$, $P_{vv} = \mathrm{Re}(\tilde{v}^*\tilde{v})$, $P_{uv} = \mathrm{Re}(\tilde{u}^*\tilde{v})$, and $Q_{uv} = -\mathrm{Im}(\tilde{u}^*\tilde{v})$, where the tilde denotes Fourier transform in time and the asterisk denotes complex conjugate. It can be shown that the rotary coefficient equals $C_0 = (S_- - S_+)/(S_- + S_+)$, where S_- and S_+ are the spectral energy in the clockwise and anticlockwise rotations of velocity vectors, respectively. The rotary coefficient C_0 is positive if the trajectory is clockwise; its magnitude is one for pure rotary motion, and zero for unidirectional motion. If the fluctuations obey linear inviscid internal-wave dynamics, Fofonoff showed that the rotary coefficient must obey the relationship

$$C_0 = \frac{2\omega f}{\omega^2 + f^2} \tag{7}$$

where ω is the *magnitude* of frequency. For $\omega \gg f$, the theoretical curve for C_0 asymptotically goes to zero since high frequency internal waves do not trace out ellipses but straight lines in the hodograph plane.

Figure 6 shows the estimates of C_0 for the Peru data, made from (6) using the observed uv-pairs at all stations. Because of the variation of f in the region, the frequency axis is normalized by plotting the variables against $\omega/|f|$. Figure 7 shows the same estimates for the CODE data, except that the frequency axis has not been normalized by f, which is practically constant in

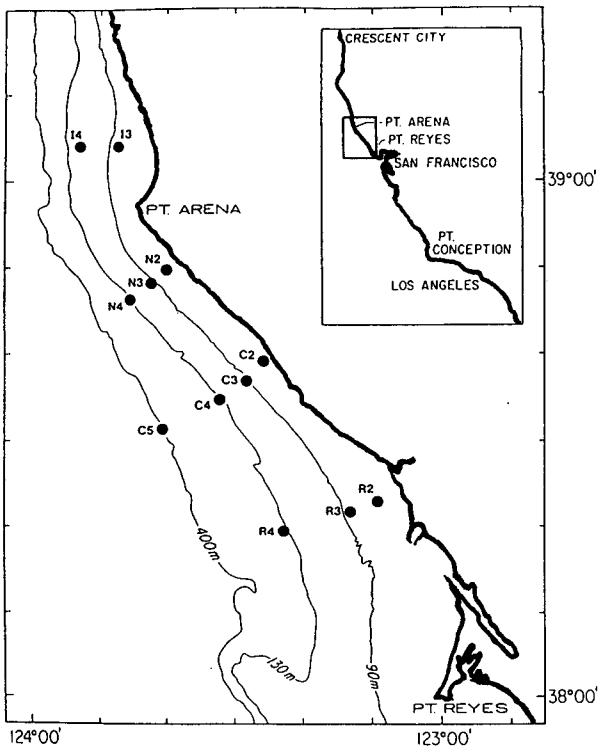

FIG. 4. Locations of current meter moorings near the coast of California during the CODE 2 experiment. Constant depth contours are indicated in meters.

the region. For both datasets, a comparison of the estimates with the theoretical curve shows some resemblance. For example, the decrease of the magnitude of C_0 with ω signifies that the elliptic particle orbits become increasingly linear. At lower frequencies the trajectories are elliptical, especially for the CODE data. The rotation is anticlockwise (C_0 negative) for the Peru data, as expected in the Southern Hemisphere. The magnitude of C_0, however, is rather small for the Peru data (latitude $\sim$ 12°S), suggesting that the internal waves are not greatly affected by planetary rotation at low latitudes. For the CODE data the rotation is clockwise, as expected in the Northern Hemisphere. The evidence of rotational effect (magnitude of C_0) is stronger at the higher latitudes of the CODE data. The conclusion is that a large part of the fluctuations in the datasets is indeed suggestive of internal wave dynamics. However, the agreement is not as good as in the open ocean data of Fofonoff, presumably due to the dominance of dissipative and nonlinear effects expected in a coastal dataset.

[Note that Fig. 13 of Kundu et al. (1988), showing only a very weak resemblance between the theoretical curve for C_0^2 and the data, is not quite correct. The source of the error was that C_0 should be estimated *after* P and Q have been averaged over band or ensemble. In Kundu et al. (1988), raw values of P and Q were used to get an estimate of a raw C_0^2, and C_0^2 was *then* band averaged. The incorrect order of averaging, coupled with squaring the raw C_0, resulted in a too large Q_{uv} at high frequencies, where the raw estimates of Q_{uv} are expected to have both signs and would cancel out on band averaging. Much of the poor agreement between the data and the theoretical curve resulted from this.]

An interesting point is that the fluctuations have a nearly 180° phase shift across the water column. This is evident from a simple vertical correlation of the current vectors at several depths on the same mooring. A more reliable way is to determine the complex vertical eigenfunctions at all stations, as described by Kundu and Allen (1976). The procedure is to determine the Hermitian matrix of complex correlation

$$R_{kj} = \overline{q^*(z_k, t)q(z_j, t)}, \quad k, j = 1, 2, \cdots, N \quad (8)$$

where $q = u + iv$ is the complex velocity, and z_k and z_j denote two depths. One then determines the complex eigenvectors ϕ_n and real eigenvalues λ_n of R_{kj}, defined by

$$\sum_{k=1}^{N} R_{kj}\phi_n(z_k) = \lambda_n\phi_n(z_j), \quad n = 1, 2, \cdots, N \quad (9)$$

The eigenvectors $\phi_n(z_j)$ represent the various empirical normal modes, and the eigenvalues denote the time-average energy (variance) in the various modes. If the eigenvalues are arranged such that $\lambda_1 > \lambda_2 > \ldots$, then the first normal mode ϕ_1 represents the dominant structure in the data. At each depth z_j, the eigenfunction ϕ_n is a complex number, and can be represented by a horizontal vector. The structure of ϕ_1 therefore shows how the horizontal fluctuations veer in depth. The advantage of the *complex* form of the empirical orthogonal modes is that both components of the horizontal velocity (u and v) can be considered simultaneously.

The vertical structure of the first empirical mode, found from the high frequency components of the horizontal velocity, is indicated in Table 3 for the Peru data, and in Table 4 for the CODE data. Since the eigenfunction can be rotated by an arbitrary amount, we have arbitrarily chosen the first element of the eigenvector (at the uppermost depth) to have zero phase angle. It is seen that the fluctuations in the surface and deep layers tend to have a nearly 180° phase shift at most stations, although there is a scatter about this behavior. Similar behavior was also found by Rosenfeld (1986) at tidal frequencies, and in many other works referenced by her. In view of the bottom slope and the dissipative effects, it is doubtful whether these are standing first modes set up by bottom reflection. A more likely reason is that friction causes a faster spatial

TABLE 2. Record-average onshore and alongshore velocity and horizontal Reynolds stress, for the CODE data.

Station–depth (m)	Distance from coast (km)	Water depth (m)	$\bar{U}$ (cm s^{-1})	$\bar{V}$ (cm s^{-1})	$\frac{\overline{uv}}{u_{rms}v_{rms}}$	$\overline{uv}$ (cm^2 s^{-2})
I3-10	10	90	−14.5	−11.8	−0.21	−4.7
I3-53			−0.7	−3.5	+0.04	+0.4
I4-10	18	130	−17.5	−12.6	−0.36	−8.7
I4-53			−1.6	−4.3	−0.19	−2.7
N2-20	3	60	1.9	−0.3	−0.06	−0.8
N3-10	6	90	−4.0	−8.0	−0.16	−3.0
N3-53			2.1	1.8	0.00	0.0
N3-83			−0.6	3.4	−0.20	−3.0
N4-10	14	130	−4.0	−12.1	−0.25	−5.5
N4-20			1.3	−8.9	−0.21	−3.2
N4-35			1.9	−6.4	−0.15	−2.0
N4-55			2.9	−2.2	−0.06	−0.6
N4-70			2.2	1.2	+0.01	+0.1
N4-90			2.3	3.9	−0.02	−0.1
N4-110			1.6	5.6	−0.12	−0.7
N4-121			1.0	6.6	−0.19	−1.4
C2-20	2	60	2.6	4.4	−0.02	−0.2
C3-5	7	90	−5.5	−6.0	−0.04	−0.6
C3-10			−4.0	−7.2	−0.14	−2.1
C3-15			−3.3	−4.2	−0.11	−1.4
C3-20			−1.4	−4.7	−0.09	−1.2
C3-35			0.5	−1.6	−0.04	−0.3
C3-53			0.8	−0.0	+0.02	+0.1
C3-70			0.2	1.1	+0.01	0.0
C3-83			0.1	0.8	−0.34	−1.8
C4-10	14	130	−8.0	−20.5	−0.19	−5.0
C4-20			−4.0	−15.8	−0.15	−2.2
C4-55			0.3	−6.9	−0.06	−0.5
C4-70			0.8	−4.4	−0.06	−0.4
C4-90			0.6	−1.4	0.00	0.0
C4-110			−0.0	−0.4	−0.20	−1.1
C4-121			0.2	1.7	−0.32	−2.6
C5-20	29	400	−0.9	−12.6	−0.16	−2.1
C5-35			1.7	−9.6	−0.19	−2.3
C5-55			3.8	−5.9	−0.21	−2.5
C5-70			4.0	−2.8	−0.16	−2.1
C5-90			3.5	0.7	−0.16	−1.6
C5-110			4.7	2.7	−0.27	−2.8
C5-150			4.3	7.5	−0.24	−2.2
C5-250			4.5	12.1	−0.19	−1.3
C5-350			3.0	7.0	−0.37	−4.2
R2-20	5	60	1.5	7.0	+0.01	+0.1
R3-20	10	90	−0.2	0.4	−0.07	−0.7
R3-53			0.9	1.6	−0.02	−0.1
R4-10	24	130	−9.1	−17.6	−0.10	−1.8
R4-20			−16.1	−22.2	−0.18	−4.7
R4-35			−5.9	−13.3	−0.02	−0.3
R4-55			−3.0	−8.2	0.00	0.0
R4-70			−1.0	−5.6	+0.01	+0.1
R4-90			0.7	−2.2	−0.06	−0.4
R4-110			−0.4	0.2	−0.28	−2.4

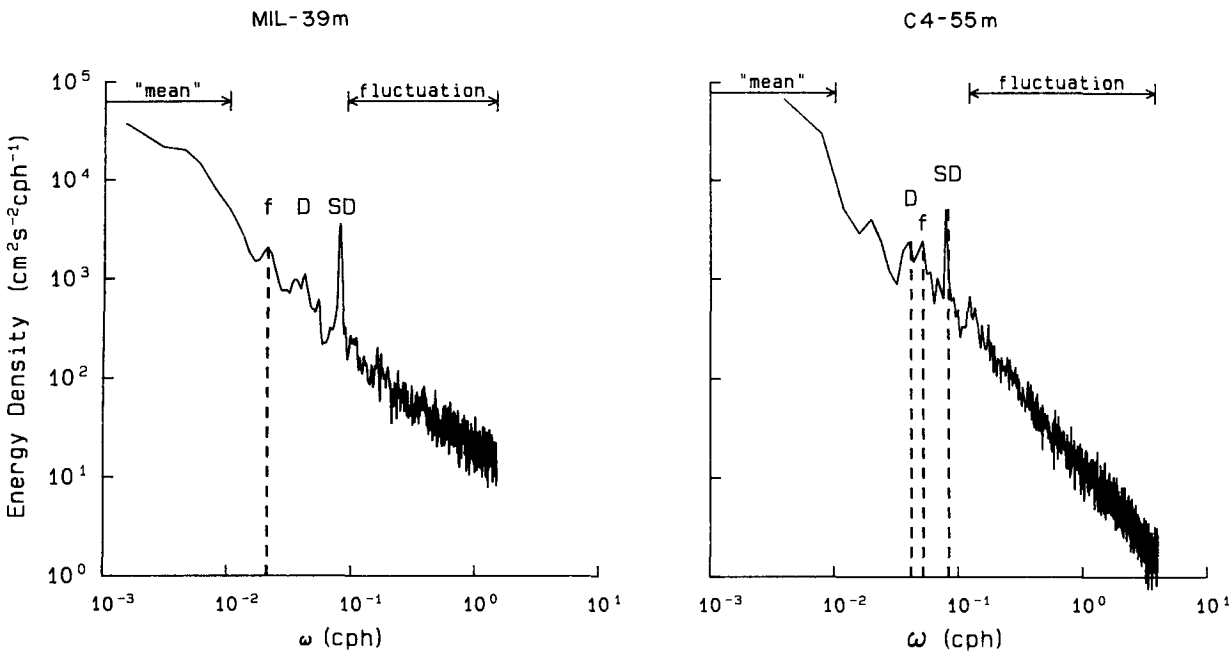

FIG. 5. Spectrum of horizontal kinetic energy at MIL-39 (Peru), and at C4-55 (CODE). The bandwidth is 0.003 cph and the degrees of freedom is 8. Diurnal, inertial and semidiurnal frequencies are respectively indicated by D, f and SD. The low and high frequency components are indicated by "mean" and "fluctuation."

decay of the higher modes from their region of generation, leaving a dominant first mode (Brink 1988).

However, the high frequency currents in CODE do not exactly display a sudden 180° phase shift in depth, but veer clockwise with depth, looking down (that is, they veer in the non-Ekman sense). This is evident from an examination of the structure of the dominant eigenfunction for the CODE data, shown in Table 4. For example, note that the phase angle at C3 varies as 3°, −6°, −15°, −31°, −118° and −158° as the depth increases from 10 to 70 m. Since the currents rotate predominantly clockwise with *time,* this means that the deeper currents are leading in phase. All CODE stations except C5 show the same behavior.

In inviscid wave theory the clockwise veering in depth, and the associated phase lead of the bottom cur-

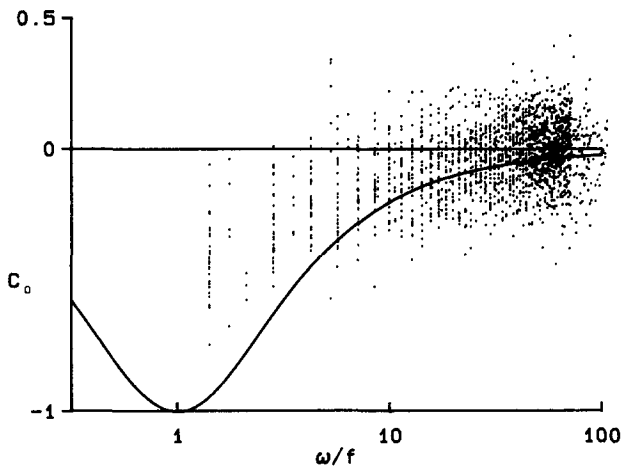

FIG. 6. Rotary coefficient of horizontal velocity components at all Peru stations, computed from equations (6). The continuous line denotes the theoretical behavior for C_0 if the fluctuations obeyed linear inviscid internal-wave dynamics. The negative C_0 signifies that the velocity vectors rotate anticlockwise. Note the presence of a weak resemblance between data and theory.

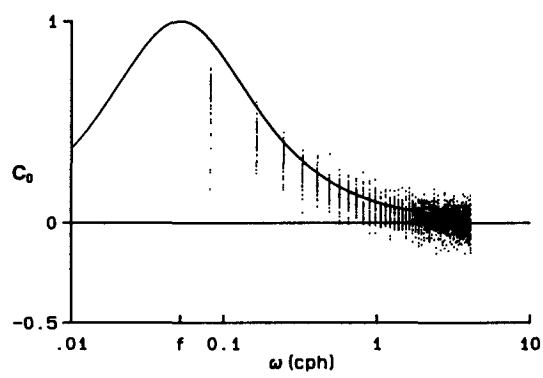

FIG. 7. Rotary coefficient of horizontal velocity components at all CODE stations, computed from equations (6). The continuous line denotes the theoretical behavior for C_0 if the fluctuations obeyed linear inviscid internal-wave dynamics. The positive C_0 signifies that the velocity vectors rotate clockwise. Note the presence of a weak resemblance between data and theory.

TABLE 3. Dominant vertical empirical mode at each station for the Peru data.

Station	First mode $\phi_1(z_j)$	Eigenvalue λ_1 (cm^2 s^{-2})	Percentage (%)
PEY-37	0.97 exp($i0°$)		
PEY-56	0.17 exp($i119°$)	20	52
PEY-96	0.18 exp($i155°$)		
AGA-26	0.99 exp($i0°$)		
AGA-46	0.05 exp($i113°$)	104	66
AGA-67	0.05 exp($i144°$)		
AGA-77	0.04 exp($i152°$)		
LOB-58	0.77 exp($i0°$)		
LOB-83	0.35 exp($i5°$)	15	37
LOB-183	0.40 exp($-i174°$)		
LOB-283	0.35 exp($-i179°$)		
LAG-92	0.59 exp($i0°$)		
LAG-115	0.55 exp($-i6°$)	13	38
LAG-224	0.59 exp($-i147°$)		
LAG-512	0.01 exp($i129°$)		
OPU-224	0.15 exp($i0°$)		
OPU-324	0.92 exp($i42°$)	12	45
OPU-524	0.37 exp($-i127°$)		
IRO-24	0.78 exp($i0°$)		
IRO-44	0.56 exp($i7°$)		
IRO-63	0.21 exp($i4°$)	65	32
IRO-105	0.23 exp($-i119°$)		
IRO-155	0.12 exp($-i178°$)		
IRO-180	0.14 exp($-i176°$)		
EUP-26	1.00 exp($i0°$)	60	61
EUP-63	0.06 exp($i64°$)		
PAR-24	0.09 exp($i0°$)		
PAR-64	0.99 exp($i169°$)	33	47
PAR-104	0.05 exp($i161°$)		
YUC-37	0.98 exp($i0°$)		
YUC-57	0.17 exp($-i8°$)	26	58
YUC-97	0.05 exp($-i125°$)		
MIL-19	0.95 exp($i0°$)		
MIL-39	0.14 exp($-i2°$)		
MIL-59	0.05 exp($-i145°$)	70	34
MIL-80	0.18 exp($i180°$)		
MIL-100	0.18 exp($i169°$)		
MIL-115	0.14 exp($i161°$)		

rents, signifies a downward propagation of energy. However, a more likely reason is frictional effects. Kundu et al. (1981) give linear solutions that describe frictional effects on periodic currents in unstratified water of finite and infinite depths. The infinite depth solution is simple and is briefly summarized here; the original paper should be consulted for details. Consider a horizontal current oscillating at a frequency ω in a homogeneous ocean, in which the frictional effects are represented by a vertical eddy viscosity ν. At the sea surface (represented by $z = \infty$) the current hodograph is assumed to be a clockwise ellipse with a semi-major axis of $(A + B)$, and a semi-minor axis of $(A - B)$. The ocean bottom is represented by $z = 0$. Defining the complex velocity $q = u + iv$, the equation of motion is

$$q_t + ifq - \nu q_{zz} = -p_x - ip_y \tag{10}$$

with the boundary conditions

$$q = 0, \quad \text{at} \quad z = 0 \tag{11}$$

TABLE 4. Dominant vertical empirical mode at each station for the CODE data.

Station	First mode $\phi_1(z_j)$	Eigenvalue λ_1 (cm^2 s^{-2})	Percentage (%)
I3-10	0.94 exp($i0°$)	36	84
I3-53	0.34 exp($-i173°$)		
I4-10	0.99 exp($i0°$)	62	73
I4-53	0.12 exp($-i122°$)		
N3-10	0.79 exp($i0°$)		
N3-53	0.14 exp($-i162°$)	38	63
N3-83	0.60 exp($-i180°$)		
N4-10	0.67 exp($i0°$)		
N4-20	0.49 exp($-i2°$)		
N4-35	0.30 exp($-13°$)		
N4-55	0.07 exp($-i105°$)	75	50
N4-70	0.17 exp($-i159°$)		
N4-110	0.24 exp($-i170°$)		
N4-121	0.28 exp($-i176°$)		
C3-5	0.43 exp($i0°$)		
C3-10	0.55 exp($i3°$)		
C3-15	0.46 exp($-i6°$)		
C3-20	0.50 exp($-i15°$)	62	54
C3-35	0.13 exp($-i31°$)		
C3-53	0.09 exp($-i118°$)		
C3-70	0.12 exp($-i158°$)		
C3-83	0.13 exp($-i156°$)		
C4-10	0.73 exp($i0°$)		
C4-20	0.48 exp($-i18°$)		
C4-55	0.11 exp($-i73°$)		
C4-70	0.12 exp($-i134°$)	79	56
C4-90	0.22 exp($-i165°$)		
C4-110	0.17 exp($i174°$)		
C4-121	0.36 exp($i174°$)		
C5-20	0.14 exp($i0°$)		
C5-35	0.27 exp($-5°$)		
C5-55	0.41 exp($-i11°$)		
C5-70	0.50 exp($-i7°$)		
C5-90	0.44 exp($-i0°$)	48	27
C5-110	0.36 exp($-i4°$)		
C5-150	0.16 exp($i20°$)		
C5-250	0.19 exp($i162°$)		
C5-350	0.34 exp($-i166°$)		
R3-20	0.98 exp($i0°$)	15	79
R3-53	0.18 exp($-i143°$)		
R4-10	0.50 exp($i0°$)		
R4-20	0.62 exp($i9°$)		
R4-35	0.39 exp($-i10°$)		
R4-55	0.18 exp($-i43°$)	88	53
R4-70	0.13 exp($-i109°$)		
R4-90	0.25 exp($-i152°$)		
R4-110	0.33 exp($-i180°$)		

$$q_z = 0, \quad \text{at} \quad z = \infty \tag{12}$$

$$q = Ae^{-i\omega t} + Be^{i\omega t}, \quad \text{at} \quad z = \infty \tag{13}$$

No generality is lost by taking A, B and ω to be positive. We shall assume that $A > B$, since then the rotation of the current ellipse is clockwise *with time,* as in the CODE data. The pressure gradient in (10) is depth independent and is known from the flow at $z = \infty$, given by (13). The solution to (10), subject to (11)–(13), can be determined by finding the homogeneous and particular solutions.

For the present dataset $\omega > f$, for which the solution is

$$q = Ae^{-i\omega t}(1 - e^{-az}e^{iaz}) + Be^{i\omega t}(1 - e^{-bz}e^{-ibz}) \tag{14}$$

where $a = \sqrt{(\omega - f)/2\nu}$ and $b = \sqrt{(f + \omega)/2\nu}$ are both positive. The term multiplied by A veers clockwise with depth (that is, *opposite* to the direction of traditional "Ekman veering" of steady flows), and the term multiplied by B veers in the opposite direction. Since $A > B$, the term multiplied by A dominates the solution. Kundu et al. (1981) showed that a similar conclusion also applies to an ocean of finite depth.

The veering between the currents at two depths, given by (14), vary during the cycle (see Fig. 10 of Kundu et al. 1981). The time-average veering between the currents q_1 and q_2 at two heights z_1 and z_2 can be computed by determining the phase angle of their complex correlation

$$R = \overline{q_1^*(t)q_2(t)} \tag{15}$$

where the overbar denotes average over a cycle. The phase angle of the complex number R is a measure of the average clockwise angle of q_1 with respect to q_2, *the averaging process being weighted according to the magnitude of the instantaneous currents.* As explained in Kundu (1976), this weighting is very appropriate for measuring the *average* veering.

In order to determine if the frictional veering described above can explain the veering observed in the CODE data, we take $f = 0.9 \times 10^{-4}$ s^{-1}, a typical value of the energetic high frequency currents as $\omega = 8 \times 10^{-4}$ s^{-1} (=0.4 cph; see the spectrum in Fig. 5b), and a typical vertical eddy viscosity as $\nu = 200$ cm^2 s^{-1}. With $z_1 = 10$ m and $z_2 = 30$ m, (15) gives a phase angle of +4.6°. Solutions show that the rate of veering is only a weak function of z, until z becomes large and comparable to the Ekman layer height $\pi\sqrt{2\nu/f}$ (see Fig. 11a of Kundu et al. 1981). For moderate heights, it follows that the model high frequency current veers clockwise with depth at an average rate of about 5° for each 20 m increase in depth. This seems to agree with the order-of-magnitude behavior in Table 4, excluding points close to the node where the veering is much sharper due to baroclinic behavior of the first mode, not considered in the homogeneous model.

We suggest that the clockwise veering (with depth) of the high frequency fluctuations in CODE is a frictional effect, rather than an effect of the downward propagation of energy. The Peru data, however, do not show any consistent veering of the fluctuating currents with depth, again suggesting that rotational effects are weak at low latitudes (see also Fig. 6).

No horizontal correlation of the high frequency series at different stations was found in the data. Consequently, horizontal maps of the empirical orthogonal functions were not computed.

4. Time variations of shear and Reynolds stress

Neither the Peru nor the CODE dataset indicate any consistent correlation of time variations of $V_x(t)$ and $\overline{uv}(t)$, or of $V_z(t)$ and $\overline{vw}(t)$. An example is shown in Fig. 8, which shows $\overline{uv}(t)$ at IRO-105 and the difference between the V at MIL-100 and IRO-105; the latter series is proportional to the time variations of V_x in the region. No correlation between the time variations of Reynolds stress and shear is apparent, and the only thing one can say is that the record-averages of the two time series have opposite signs. Such behavior was found nearly at all stations in both datasets. Therefore, it is only on time scales longer than several weeks that the two series may have a relationship. This is indeed the case, as will be discussed later.

As with the horizontal shear, no consistent correlation of the vertical Reynolds stress $\overline{vw}(t)$ and vertical shear $V_z(t)$ was found in either dataset. Even the record averages $\overline{vw}$ and $\overline{V}_z$ did not have opposite signs. The probable reason for such a behavior is discussed in section 8.

5. Record-average behavior of mean shear and Reynolds stress

We now examine whether there is any relationship between the shear and Reynolds stresses, when aver-

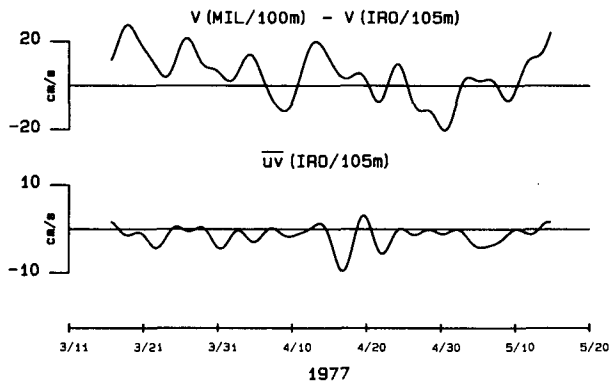

FIG. 8. Comparison of time variations of $\overline{uv}$ at 100 m on mooring Ironwood, and the difference of V at MIL-100 and IRO-105. Note the lack of correlation.

aged over the *entire* record length (2–3 months for the Peru data and 4–5 months for the CODE data). As mentioned previously, these averages are indicated by a double overbar. The average alongshore and onshore velocity components for the two datasets are listed in Tables 1 and 2. Except for a few surface locations in the CODE region, the values of $\bar{\bar{U}}$ are smaller than those of $\bar{\bar{V}}$, suggesting that the horizontal strain rate field is dominated by $\bar{\bar{V}}_x$, as assumed in (3).

For the Peru data, the mean values of $\bar{\bar{V}}$ on a cross-shore section through Agave–Lobivia are indicated in Fig. 9. It is seen that $\bar{\bar{V}}$ is southward everywhere. Near the coast the decrease of speed suggests a "no-slip condition" at the coast, and $\bar{\bar{V}}_x > 0$. Away from the coast, $\bar{\bar{V}}_x$ is nearly zero, or slightly negative. At PEY, PAR and OPU, the sign of $\bar{\bar{V}}_x$ cannot be estimated due to lack of data at several values of x for the same z. However, Table 1 shows that $\bar{\bar{V}}$ is negative at these stations, and $\bar{\bar{V}}_x$ should be positive at least near the coast because of the no-slip condition.

For the CODE data, offshore variations of $\bar{\bar{V}}$ along the I and C lines are shown in Fig. 10. The variation along the N line is roughly similar to that along the I line, and the variation along the R line is very similar to that along the C line (Table 2). Offshore, the flow is generally southward, the surface flow being stronger. Inshore, the surface flow is sometimes northward

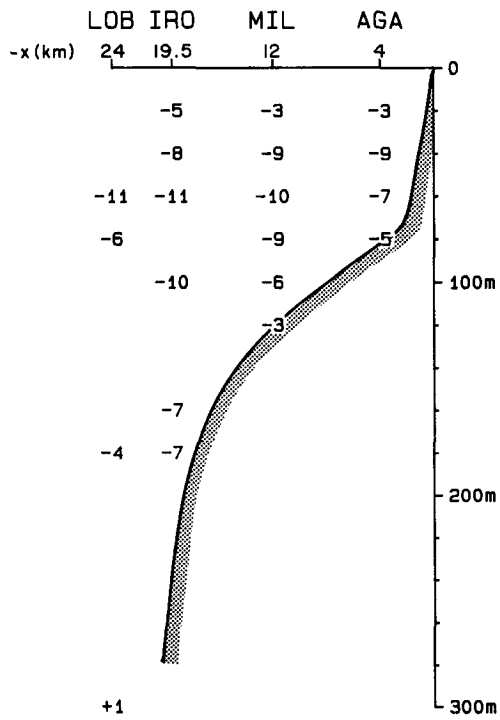

FIG. 9. Mean alongshore velocity (cm s^{-1}) on a cross section through the Peru stations Agave, Mila, Ironwood and Lobivia. The mean shear is positive nearshore, and negligible away from the coast.

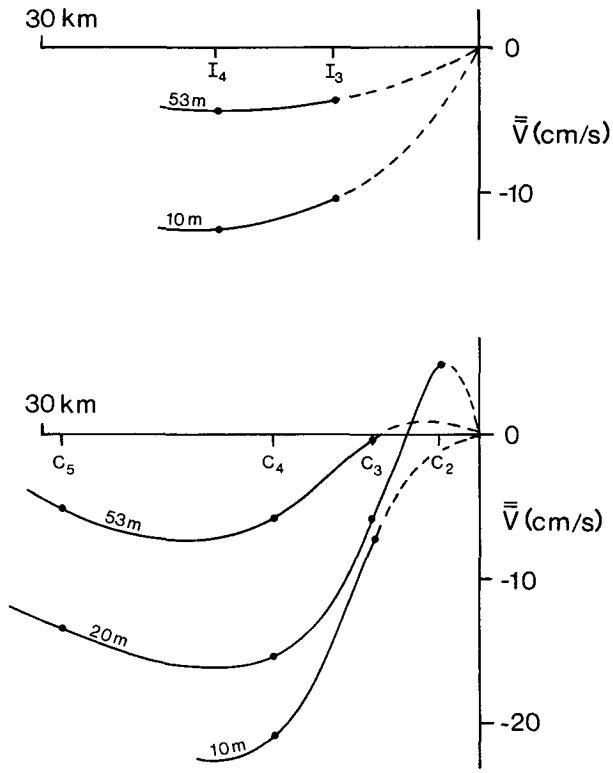

FIG. 10. Offshore distributions of mean alongshore velocity along the I and C lines of CODE data. The mean shear is generally positive, except far offshore and sometimes next to the coast.

("counter-current") due to occasional wind relaxation events (Send et al., 1987). It is seen that the horizontal shear $\bar{\bar{V}}_x$ changes sign along several offshore lines in the CODE region, as in the British Columbia data (Fig. 2). As we shall see, the change in the sign of local shear is not associated with a change in the sign of the Reynolds stress.

The record-average horizontal Reynolds stresses are almost always negative. This is indicated in Table 1 for the Peru data, and Table 2 for the CODE data. These tables list the correlation coefficient

$$r = \frac{\overline{\overline{uv}}}{u_{\text{rms}} v_{\text{rms}}}$$

It is seen that, for both datasets, the sign of the Reynolds stress is usually negative everywhere, whatever the sign of the local strain rate $\bar{\bar{V}}_x$. The correlation coefficients are not very high, but the magnitudes larger than 0.14 are significant at the 95% level. [The high frequency fluctuations were found to have a decorrelation length of about 8 hours for the Peru data. For a record length of 70 days the number of independent measurements is therefore 210. This gives a 95% significance level of 0.14. A similar significance level was also found for the CODE data.] Besides, the correlation is not ex-

pected to be high for several reasons. First, the particle orbits are expected to be ellipses, and not straight lines. In such a case a perfect correlation is not possible even if the orbital axes were of unchanging orientation, that is, if the propagation direction of the waves remained constant in time. Second, if a local correlation did hold, for a positive eddy viscosity the time-varying Reynolds stress would change sign when the shear rate $V_x(t)$ changes sign, resulting in a low record-average correlation $\overline{uv}$. Moreover, the low values of correlation lead to values of Reynolds stresses that are consistent with commonly used values of eddy viscosity, as we shall see in the next section.

Some of the scatter plots of the high frequency u and v are shown in Fig. 11 for the Peru data, and in Fig. 12 for the CODE data. The principal axes are seen to be inclined at a large angle to the x and y axes, so that the nonzero Reynolds stress could not result from

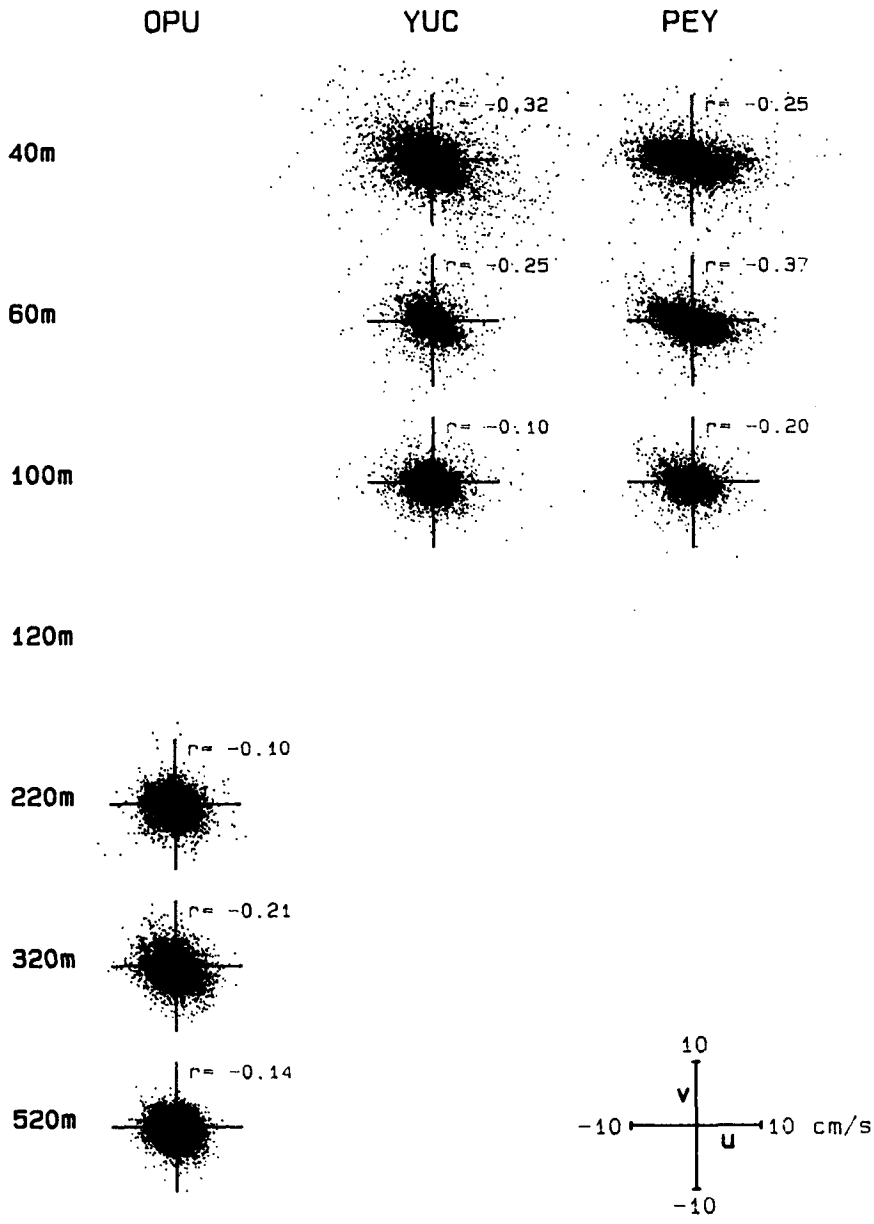

FIG. 11. Scatter plots of high frequency fluctuations u versus v at the Peru stations Opuntia, Yucca and Peyote, over the entire record. The velocity scale is shown in the lower right-hand corner. The correlation coefficient r between u and v is recorded alongside each plot. Note that r is negative everywhere.

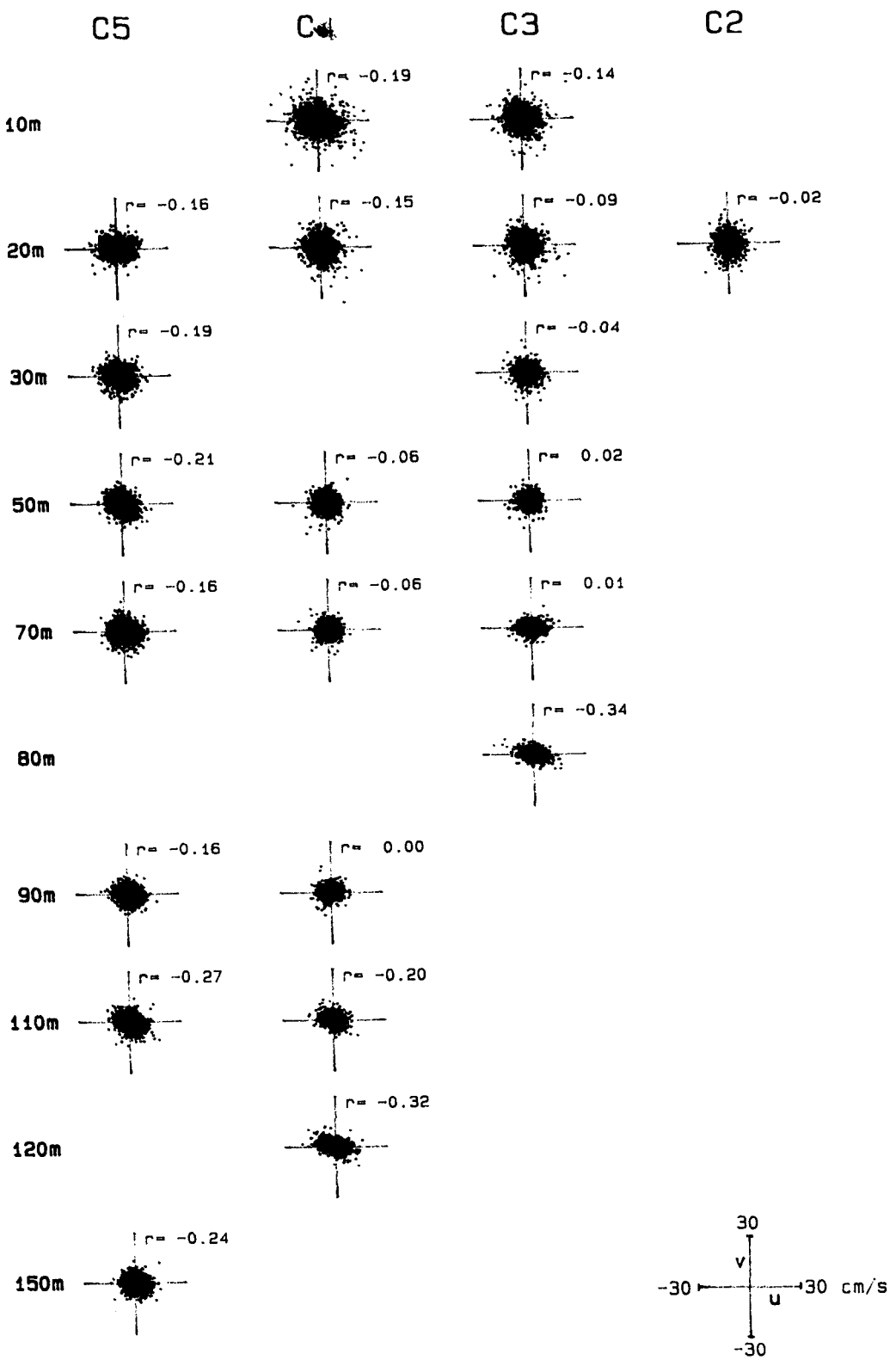

FIG. 12. Scatter plots of high frequency fluctuations u versus v at the CODE stations along the C line, over the entire record. The velocity scale is shown in the lower right-hand corner. The correlation coefficient r between u and v is recorded alongside each plot. Note that r is negative almost everywhere.

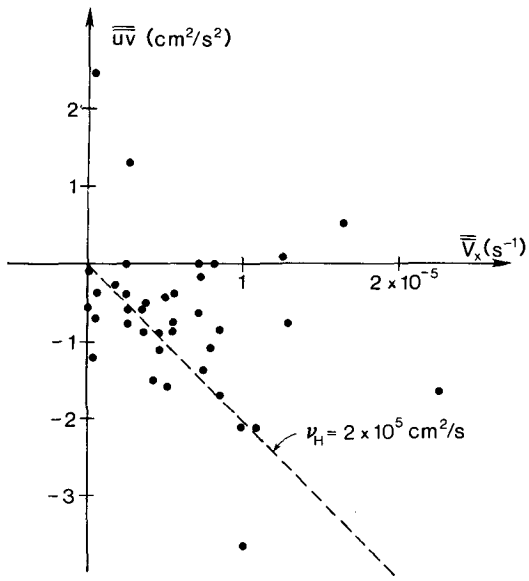

FIG. 13. Record-average values of horizontal Reynolds stress, plotted against average $\bar{\bar{V}}_x$ each station estimated as $-\bar{\bar{V}}/\Delta x$, where Δx is the distance from the coast. Note the negative correlation.

an erroneous estimate of the orientation of the alongshore coordinate.

It is interesting that the record-mean $\bar{\bar{V}}$ and $\overline{\overline{uv}}$ are negatively correlated for the Peru data, as can be seen by comparing their values in Table 1. This may be a reflection of the fact that large $\bar{\bar{V}}$ in the surface layers corresponds to large values of an average $\bar{\bar{V}}_x$ at these depths. In order to pursue this idea, we estimate a region-average $\bar{\bar{V}}_x$ from the local values of $\bar{\bar{V}}$. A rough estimate of a region-average $\bar{\bar{V}}_x$ at a certain location can be obtained by taking the difference between the coastal value of $\bar{\bar{V}}(=0)$ and the local $\bar{\bar{V}}$ at that location; this is the average shear as seen by a wave packet going across the shelf. The average shear at a station is therefore estimated as

$$\bar{\bar{V}}_x \sim \frac{0-\bar{\bar{V}}}{\Delta x} = -\frac{\bar{\bar{V}}}{\Delta x}$$

where Δx is the distance of the station from the coast. This rough measure of shear is plotted in Fig. 13 against the corresponding $\overline{\overline{uv}}$ at the station. It shows that there is a negative correlation between the region-average $\bar{\bar{V}}_x$ and $\overline{\overline{uv}}$, and the regression line gives a horizontal eddy viscosity of $\nu_H \sim 2 \times 10^5$ cm^2 s^{-1}. The CODE data does not support a similar observation, but an order of magnitude estimate of $\nu_H \sim 10^5$ cm^2 s^{-1} is suggested from the fact that $\overline{\overline{uv}}$ is of order -1 cm^2 s^{-1}, while $\bar{\bar{V}}_x$ is of order (20 cm s^{-1}/20 km) $= 10^{-5}$ s^{-1}. The values of ν_H suggested from these data are somewhat smaller than the eddy coefficients $\nu_H \sim 10^6$ s^{-1} commonly used in numerical models. The smaller values are expected here because only a range of high frequencies are retained within the fluctuations.

The vertical Reynolds stresses $\overline{\overline{uw}}$ and $\overline{\overline{vw}}$ are found to be negligible everywhere, except deep in the water column near the shelf break, such as OPU-520 and LAG-520 for Peru data and C5-250 and C5-350 for CODE data, where the data showed $\overline{\overline{uw}} > 0$ and $\overline{\overline{vw}} < 0$. For example, at C5-350 we found $\overline{\overline{uw}}/(u_{\rm rms}w_{\rm rms}) = 0.34$ and $\overline{\overline{vw}}/(v_{\rm rms}w_{\rm rms}) = -0.19$. The positive value of $\overline{\overline{uw}}$ at these locations seems to be due to the steeply sloping bottom, where a positive u results in a positive w. The negative value of $\overline{\overline{vw}}$ then follows, because $\overline{\overline{uv}} < 0$ and $\overline{\overline{uw}} > 0$ requires $\overline{\overline{vw}} < 0$. A similar behavior was also found in Kundu et al. (1988). Also consistent with Kundu et al. (1988), no relation is found between the vertical shear $\bar{\bar{V}}_z$ and the vertical Reynolds stress $\overline{\overline{vw}}$.

6. Summary and discussion

Two coastal datasets have been analyzed to explore if there is any relationship between the Reynolds stress generated by the high frequency motion ($0.092 < \omega < 1.5$ cph for Peru data and $0.125 < \omega < 4.0$ cph for CODE data), and the shear of the low frequency motion ($\omega < 0.01$ cph). A part of the high frequency components is consistent with internal wave dynamics (Figs. 6 and 7). The rather weak nature of agreement in these two figures, however, implies that large parts of the high frequency fluctuations are inconsistent with the behavior of internal waves, suggesting that they are affected by dissipative, generative and nonlinear processes, as expected in coastal areas. The phase of the high frequency motion changes by nearly 180° across the water column (Tables 3 and 4), suggesting the domination of the first baroclinic mode. This is presumably the result of frictional decay of the higher modes. In the CODE data there is also consistent evidence of upward phase propagation and the associated clockwise veering of the currents with depth (Table 4). This could result from a downward energy propagation and surface forcing, but a more plausible explanation is vertical frictional effects (Kundu et al. 1981).

No relationship is found between the time variations of horizontal Reynolds stress $\overline{\overline{uv}}(t)$ and the horizontal shear $V_x(t)$. When averaged over the entire record, almost always the average horizontal stress $\overline{\overline{uv}}$ is either negative or negligible (Tables 1 and 2). For the Peru data, the record-average shear $\bar{\bar{V}}_x$ is positive immediately next to the coast, and negligible or slightly negative offshore (Fig. 9 and Table 1). For the CODE data, the record-average $\bar{\bar{V}}_x$ next to the coast is negative at a few locations due to the existence of a countercurrent (Fig. 10). An overall value of $\bar{\bar{V}}_x$, obtained by averaging across the shelf for several tens of kilometers, is however positive for both datasets. It therefore appears that there is an overall negative correlation between the horizontal shear and Reynolds stress, when averaged over a region large enough in time and space.

With this picture in mind, it is possible to explain the record-average behavior of the Reynolds stress and shear field in the present datasets, as well as in Kundu et al. (1988). Let us consider the mean velocity field in Fig. 2, where the shear changes sign across the shelf. Suppose that the relaxation time, during which the internal wave packets lose their coherence, anisotropy and asymmetry, is in the neighborhood of $\tau_R \sim 2$–5 days; this estimate is consistent with the value of $\tau_R \sim 200$ hours predicted by Olbers (1976). With a typical horizontal group speed of 10 cm s^{-1} (Briscoe 1983, Müller 1977), they can then propagate across the shelf for distance of order 20–50 km, and cause momentum exchange between different regions. The presence of coherent cross-shelf currents would also aid in the propagation of the internal waves across the shelf. Recent satellite observations (for example, Kosro and Huyer 1986; Flament et al. 1985) indicate the ubiquitous presence of squirts or filaments that stretch across the coastal zone for distances of order 100 km, with associated cross-shelf motion. Higher frequency fluctuations, say, due to the internal waves, would be embedded on this motion, and would therefore propagate across the entire shelf. Although the time scale of the eddies is slow ($\sim$10 days), they can transport high frequency fluctuations across the entire shelf by simply advecting them along.

In this scenario, it is no longer necessary for the internal wave packets to be oriented at a specific angle with the local mean shear field, as suggested by Kundu et al. (1988) where a *local* correlation between Reynolds stress and mean shear was speculated. It is only necessary for a coherent signal to propagate across the shear field and transport momentum. The fact that no significant horizontal correlation between the simultaneous velocity fluctuations was found in the data does not violate this scenario. First, the fluctuating motion takes a few days to propagate across the shear field, so that the zero-lag correlations are not expected to be high. Second, even the time-lagged correlations are not expected to be significant, because the fluctuations at a point are made up of signals coming from various sources, resulting in phase mixing. This is especially true in a coastal region, in which multiple reflections are possible.

The net effect would be that mean momentum will be transported across the entire profile in Fig. 2. For example, wave packets traveling from T2 to T4 would generate a positive v (and therefore a negative $\overline{uv}$) at T4. Similarly, wave packets traveling from T4 to T2 would generate a negative $\overline{uv}$ at T2. The momentum flux at T2 is *up* the local velocity gradient, and the behavior there is as if the local eddy viscosity were negative. The anomalous behavior is a reflection of the fact that the length scale of the fluctuating motion ("mixing length") is larger than the scale of curvature of mean velocity profile. When averaged over the entire shelf, however, the behavior would be consistent with a positive eddy viscosity. A similar argument shows that the mean profiles of the present datasets (Figs. 9 and 10) should generate negative Reynolds stress.

No consistent behavior, however, is found to indicate that the same behavior is also true for the vertical Reynolds stress. Ruddick and Joyce (1979) and Kundu et al. (1988) also failed to notice any consistent behavior of the vertical Reynolds stress. It is unclear whether this is due to the errors involved in estimating the vertical velocity. A more likely reason is that the relaxation time is larger than the propagation time in the vertical, because of the shallow water depth. With a typical depth of 100 m and a typical vertical group speed of 1 cm s^{-1}, the propagation time is 3 h, much smaller than the relaxation time. Evidence of the first vertical mode also strongly supports this idea.

The correlation coefficient $\overline{uv}/(u_{\text{rms}}v_{\text{rms}})$ is found to be small. However, *three* independent datasets [Peru and CODE sets here, and the British Columbia set in Kundu et al. (1988)] behaved in a very similar manner. Collectively, then, it is convincing that the fluctuating horizontal motion, when averaged over large enough space and time, does extract energy from the low frequency motion, and act as positive horizontal eddy viscosity. An overall value of eddy viscosity generated by the high frequency fluctuation retained here is found to be $\nu_H \sim 10^5$ cm^2 s^{-1}. When the frequency range is expanded, the effective viscosity on the mean flow is expected to be larger.

Acknowledgments. Pijush Kundu was supported by NSF Grant OCE-87-09705, Robert Beardsley was supported by NSF Grant OCE-87-16937, and Adriana Huyer was supported by NSF Grant OCE-87-09930. We thank Clinton Winant and Russ Davis for sending us the CODE data, Kevin Kohler for programming help, and Kathy Maxon for the drafting.

REFERENCES

Brink, K. H., 1988: On the effect of bottom friction on internal waves. *Contin. Shelf Res.*, **8**, 397–403.

Enfield, D. B., R. L. Smith and A. Huyer, 1978: A compilation of observations from moored current meters. Oregon State University Data Rep. 70, Ref. 78-4.

Flament, P., L. Armi and L. Washburn, 1985: The evolving structure of an upwelling filament. *J. Geophys. Res.*, **90**, 11 765–11 778.

Fofonoff, N. P., 1969: Spectral characteristics of internal waves in the ocean. *Deep-Sea Res.*, **16**, 58–71.

Frankignoul, C., 1974: Observed anisotropy of spectral characteristics of internal waves induced by low-frequency currents. *J. Phys. Oceanogr.*, **4**, 625–634.

——, 1976: Observed interaction between oceanic internal waves mesoscale eddies. *Deep-Sea Res.*, **23**, 805–820.

——, and T. M. Joyce, 1979: On the internal wave variability during the internal wave experiment (IWEX). *J. Geophys. Res.*, **84**, 769–776.

Gonella, J., 1972: A rotary-component method for analyzing meteorological and oceanographic vector time series. *Deep-Sea Res.*, **19**, 833–846.

Kosro, P. M., and A. Huyer, 1986: CTD and velocity surveys of seaward jets off northern California, July 1981 and 1982. *J. Geophys. Res.*, **91,** 7680–7690.

Kundu, P. K., 1976: Ekman veering observed near the ocean bottom. *J. Phys. Oceanogr.*, **6,** 238–242.

——, and J. S. Allen, 1976: Some three-dimensional characteristics of low frequency current fluctuations near the Oregon coast. *J. Phys. Oceanogr.*, **6,** 181–199.

——, J. O. Blanton and M. M. Janopaul, 1981: Analysis of current observations on the Georgia shelf. *J. Phys. Oceanogr.*, **11,** 1139–1149.

——, R. E. Thomson, B. M. Hickey and P. H. LeBlond, 1988: Interaction of internal waves and mean flow observed near a coast. *J. Mar. Res.*, **46,** 1–23.

Muller, P., 1976: On the diffusion of momentum and mass by internal waves. *J. Fluid Mech.*, **77,** 789–823.

——, 1977: Spectral features of the energy transfer between internal waves and a large scale shear flow. *Dyn. Atmos. Oeans,* **2,** 49–72.

Olbers, D. J., 1976: Non-linear energy transfer and the energy balance of the internal wave field in the deep ocean. *J. Fluid Mech.*, **74,** 375–399.

Rosenfeld, L., 1986: Tidal band current variability over the northern California continental shelf. Ph.D. thesis, Woods Hole—Massachusetts Institute of Technology Joint Program.

Ruddick, B. R., and T. M. Joyce, 1979: Observations of interaction between the internal wavefield and low-frequency flows in the Atlantic. *J. Phys. Oceanogr.*, **9,** 498–517.

Send, U., R. C. Beardsley and C. D. Winant, 1987: Relaxation from upwelling in CODE. *J. Geophys. Res.*, **92,** 1683–1698.

Winant, C. D., U. Send and S. J. Lentz, 1985: CODE-2: Moored current observations. *CODE-2: Moored Array and Large-Scale Data Report,* R. Limburner, Ed., WHOI Tech. Rep. 85-35, 232 pp.

——, R. C. Beardsley and R. E. Davis, 1987: Moored wind, temperature, and current observations made during CODE-1 and CODE-2 over the northern California continental shelf and upper slope. *J. Geophys. Res.*, **92,** 1569–1604.